CELL BIOLOGY

A non-immunological role for γ-interferon–inducible lysosomal thiol reductase (GILT) in osteoclastic bone resorption

Benjamin W. Ewanchuk[1,2], Corey R. Arnold[1,2], Dale R. Balce[3], Priyatha Premnath[4], Tanis L. Orsetti[1], Amy L. Warren[5], Alexandra Olsen[4], Roman J. Krawetz[4], Robin M. Yates[1,2,3]*

The extracellular bone resorbing lacuna of the osteoclast shares many characteristics with the degradative lysosome of antigen-presenting cells. γ-Interferon–inducible lysosomal thiol reductase (GILT) enhances antigen processing within lysosomes through direct reduction of antigen disulfides and maintenance of cysteine protease activity. In this study, we found the osteoclastogenic cytokine RANKL drove expression of GILT in osteoclast precursors in a STAT1-dependent manner, resulting in high levels of GILT in mature osteoclasts, which could be further augmented by γ-interferon. GILT colocalized with the collagen-degrading cysteine protease, cathepsin K, suggesting a role for GILT inside the osteoclastic resorption lacuna. GILT-deficient osteoclasts had reduced bone-resorbing capacity, resulting in impaired bone turnover and an osteopetrotic phenotype in GILT-deficient mice. We demonstrated that GILT could directly reduce the noncollagenous bone matrix protein SPARC, and additionally, enhance collagen degradation by cathepsin K. Together, this work describes a previously unidentified, non-immunological role for GILT in osteoclast-mediated bone resorption.

INTRODUCTION

The dynamic nature of bone is necessary for normal growth, repair, and calcium homeostasis and requires a fine balance of bone synthesis and bone resorption. While the mesenchymal stem cell–derived osteoblasts synthesize new bone, the myeloid-derived osteoclasts are ultimately responsible for the resorption of bone (*1*). Dysregulation of bone turnover can lead to a net loss or net gain of bone density, resulting in osteoporosis or osteopetrosis, respectively. While the pathogenesis of osteoporosis is multifactorial, osteoclast dysfunction is principally blamed for the development of osteopetrosis (*2*).

Unique among tissue-resident macrophage populations, osteoclasts are giant multinucleated cells formed via the fusion of embryonic and hematopoietic stem cell precursors of erythromyeloid and myeloid lineages (*3*–*6*). The survival/proliferation and differentiation of osteoclasts are driven by the cytokines macrophage colony-stimulating factor (M-CSF; also known as CSF-1) and receptor activator of nuclear factor κB ligand (RANKL; also known as TNFSF11), respectively (*7*, *8*). Once mature, osteoclast $\alpha_V\beta_3$ integrins adhere to organic bone matrix to form a tight sealing zone against the surface of the bone, resulting in an isolated extracellular compartment termed the resorption lacuna. Vacuolar (V-)ATPase proton pumps at the ruffled border of the lacuna serve to acidify the compartment, and polarized lysosomal secretion deposits numerous lysosomal proteins within the resorption lacuna including acid phosphatases, matrix metalloproteinases (MMPs), and lysosomal cysteine cathepsins (*9*–*13*). The end result is an acidic, highly degradative compartment optimized for the resorption of the inorganic and organic components of bone. Cathepsin K is the major protease within the resorption lacunae of osteoclasts and is principally charged with the degradation of collagen (*12*, *14*). In humans, an autosomal recessive deficiency in cathepsin K results in pycnodysostosis, a severe osteopetrotic phenotype further modeled in mice following genetic deletion of cathepsin K (*15*–*17*). Similar to other lysosomal cysteine protease members, cathepsin K has an acidic optimum, and the active site cysteine must remain in a reduced thiol state for protease activity (*18*).

γ-Interferon–inducible lysosomal thiol reductase (GILT) remains the sole reductase described within vesicles of the endolysosomal system of mammalian cells (*19*, *20*). Predominantly studied in the context of antigen presentation, GILT directly catalyzes the reduction of disulfide bonds, which has been shown to be a requirement for the processing of a variety of self-, infectious, and neoplastic protein antigens containing inter- or intramolecular disulfides (*21*–*25*). More recently, it has been found that GILT is also required for optimal activity of the lysosomal cysteine protease, cathepsin S, in alternatively activated macrophages—presumably, through maintaining the active-site cysteine in its thiol state within the acidic environment of the lysosome (*18*, *26*). Despite evidence that the evolution of GILT preceded that of the adaptive immune system, functions for GILT beyond its well-defined role in antigen processing remain mostly unexplored (*27*–*30*).

In contrast to cytosolic thioreductases such as thioredoxin, GILT has an acidic pH optimum for activity (*19*). The acidified, lysosomal content–rich resorption lacuna of the osteoclast thus offers an ideal microenvironment for GILT activity; however, expression and corresponding function of GILT within osteoclasts were previously uncharacterized. Herein, a key role for GILT in the maintenance of the bone resorptive capacity of osteoclasts is described. We found that the osteoclastogenic cytokine RANKL is a strong inducer of GILT expression, and genetic deletion of GILT significantly impaired bone resorption efficiency in vivo and in vitro. Additional evidence suggests that GILT contributes to bone resorption within the resorption lacuna via direct reduction of noncollagenous bone protein and the maintenance of proteolysis by the cysteine protease

[1]Calvin, Phoebe and Joan Snyder Institute for Chronic Diseases, Cumming School of Medicine, University of Calgary, Calgary, AB T2N 4N1, Canada. [2]Department of Biochemistry and Molecular Biology, Cumming School of Medicine, University of Calgary, Calgary, AB T2N 4N1, Canada. [3]Department of Comparative Biology and Experimental Medicine, Faculty of Veterinary Medicine, University of Calgary, Calgary, AB T2N 4N1, Canada. [4]Department of Cell Biology and Anatomy, Cumming School of Medicine, University of Calgary, Calgary, AB T2N 4N1, Canada. [5]Department of Veterinary Clinical and Diagnostic Sciences, Faculty of Veterinary Medicine, University of Calgary, Calgary, AB T2N 4N1, Canada.
*Corresponding author. Email: rmyates@ucalgary.ca

cathepsin K. Collectively, this report identifies a previously unknown non-immunological role for GILT in osteoclastic bone resorption.

RESULTS

RANKL up-regulates GILT expression in a STAT1-dependent fashion

To evaluate expression of GILT in osteoclasts, M-CSF and RANKL, or M-CSF alone, were used to drive differentiation of murine bone marrow–derived monocytic precursors to osteoclasts and bone marrow–derived macrophages (BMMØs), respectively. At both the transcript and protein levels, GILT expression was significantly increased in RANKL-treated osteoclasts compared with BMMØs (Fig. 1, A and B). By immunofluorescence, GILT was found to be highly expressed in multinucleated as well as individual mononuclear cells stimulated with M-CSF and RANKL (Fig. 1C and fig. S1). In large multinucleated osteoclasts, GILT was found to colocalize with the lysosomal cysteine protease, cathepsin K (Pearson's correlation coefficient, 0.703 ± 0.07) (Fig. 1C and fig. S1). Similar to its expression in antigen-presenting cells (APCs) (*19*, *31*, *32*), RANKL-driven

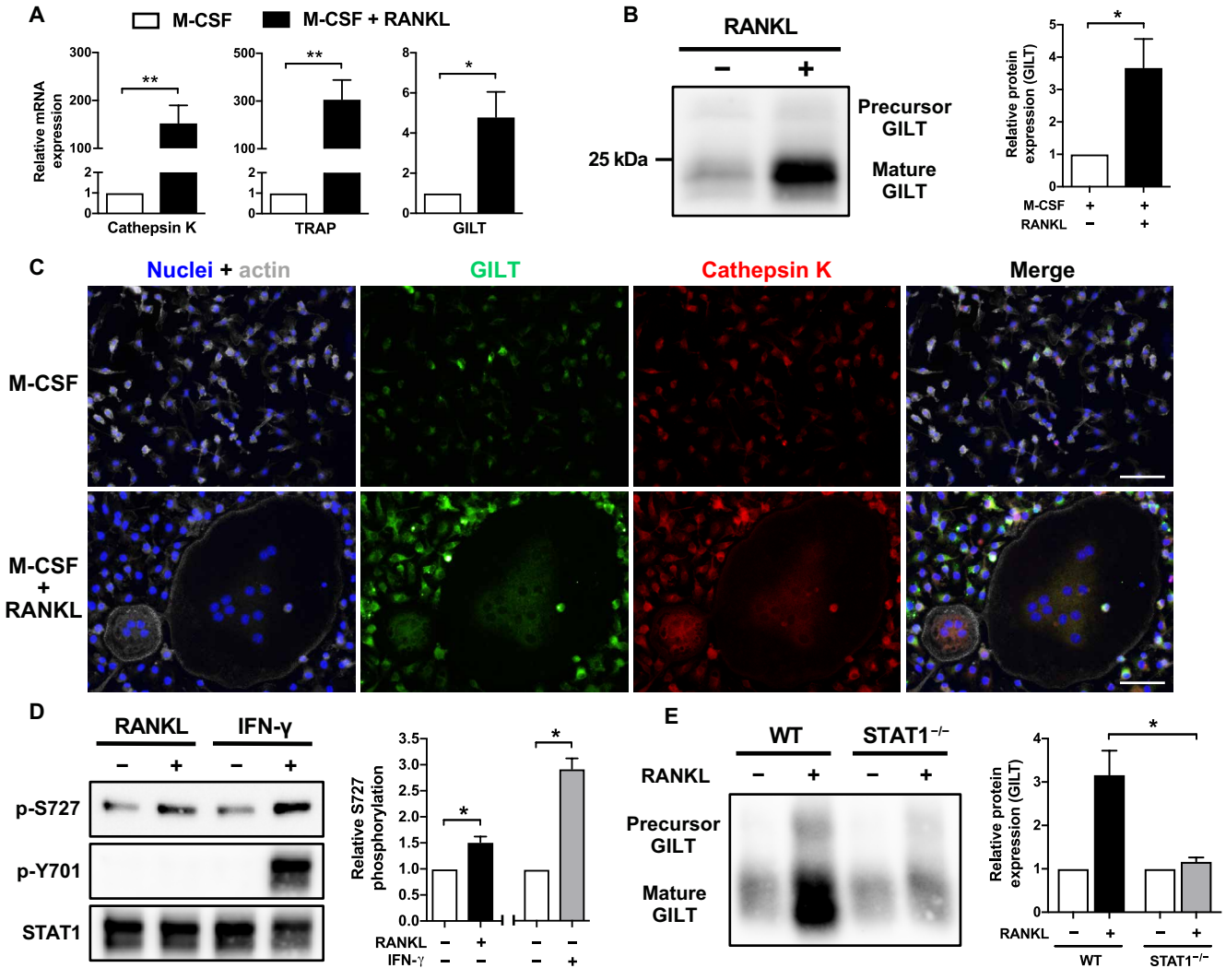

Fig. 1. RANKL induces GILT expression in a STAT1-dependent manner. (**A**) mRNA expression of the osteoclast markers cathepsin K and tartrate-resistant acid phosphatase (TRAP), as well as GILT in M-CSF–stimulated WT bone marrow cells treated with or without RANKL as measured by quantitative polymerase chain reaction (qPCR) ($n = 8$ to 9). Expression was normalized to 18*S* ribosomal RNA and made relative to M-CSF control samples. (**B**) Representative Western blot image depicting GILT protein levels following lysis of WT BMMØs (–RANKL) or osteoclasts (+RANKL). Mature GILT expression was normalized to total protein levels ($n = 5$). (**C**) Detection of GILT (green) and cathepsin K (red) by immunofluorescence microscopy in BMMØs (M-CSF) or osteoclasts (M-CSF + RANKL). Scale bars, 50 μm. Colocalization of the GILT and cathepsin K signals was assessed by calculating the Pearson's correlation coefficient in BMMØs (0.743 ± 0.04) and osteoclasts (0.703 ± 0.07) ($n = 3$ to 4 images). (**D**) STAT1 phosphorylation status within WT osteoclast precursors left untreated (–) or treated for 15 min (+) with RANKL (200 ng/ml) or IFN-γ (100 U/ml). Levels of phosphorylation were normalized to total STAT1 levels and made relative to untreated controls ($n = 3$). (**E**) GILT protein expression by WT or STAT1$^{-/-}$ osteoclast precursors following 48-hour treatment with M-CSF + RANKL (15 ng/ml + 100 ng/ml) or M-CSF only. Mature GILT levels were normalized to total protein levels and made relative to M-CSF–only controls ($n = 3$). (A to C) Cells were differentiated for 6 days with M-CSF (15 ng/ml) and RANKL (100 ng/ml), or M-CSF (15 ng/ml) only, throughout the entirety of each experiment. (D and E) Precursor cells were expanded in M-CSF (15 ng/ml) for 48 hours before described treatments. (A to E) Error bars are presented as means ± SEM. *$P < 0.05$, **$P < 0.01$ by paired (A to D) or unpaired (E) Student's *t* test.

expression of GILT could be further augmented in mature osteoclast populations with interferon-γ (IFN-γ) (fig. S2, A and B).

IFN-γ–driven expression of GILT is dependent on signal transducer and activator of transcription 1 (STAT1) signaling (*32*). Because RANKL results in phosphorylation of STAT1 at serine-727 (S727) during osteoclast differentiation (*33*), we evaluated whether STAT1 is required to induce GILT expression in response to RANKL. RANKL treatment of M-CSF–derived monocytic precursors led to phosphorylation of STAT1 at S727, but not tyrosine-701 (Y701), whereas IFN-γ led to robust phosphorylation of STAT1 at both S727 and Y701, as previously reported (Fig. 1D). Consistent with the involvement of STAT1, the ability of RANKL to drive GILT expression in monocytic precursors from STAT1-deficient mice was significantly compromised (Fig. 1E). Collectively, these findings identify the osteoclastogenic cytokine RANKL as a potent activator of GILT expression mediated through a STAT1-dependent pathway. The high levels of GILT in mature osteoclasts, and its colocalization with cathepsin K, led us to investigate a potential functional role for the reductase in bone resorption.

GILT-deficient mice exhibit an osteopetrotic phenotype

On the basis of the reported function of GILT in lysosomes of APCs, we hypothesized that GILT may function to maintain the proteolytic capacity of osteoclasts and, accordingly, play a role in bone resorption. To assess the influence of GILT activity on bone turnover in vivo, we quantified bone parameters of tibiae of 20-week-old female wild-type (WT) and GILT-deficient mice by microcomputed tomography (μCT). Tibiae from GILT$^{-/-}$ animals exhibited significant increases in both cortical and trabecular bone mineral density (10 and 29%, respectively), as well as trabecular bone volume ratio (35%) compared with WT controls (Fig. 2, A to D). A discernable, albeit insignificant increase in trabecular connective density (34%) was also observed ($P = 0.091$) (Fig. 2E). Histological analysis likewise revealed increased trabecular bone within the tibiae of 20-week-old female GILT$^{-/-}$ mice compared with WT, despite equal numbers of mature osteoclasts (Fig. 2, F to H). In addition, serum concentrations of the collagen breakdown product CTX-I, but not the bone formation biomarker PINP (N-terminal propeptide of type I procollagen), were significantly decreased in GILT$^{-/-}$ mice, suggesting impaired bone resorption, but not bone formation, in these animals (Fig. 2, I and J). To determine whether these changes modified the biomechanical properties of the bone, tibiae from WT and GILT$^{-/-}$ mice were compared by three-point flexural testing (Fig. 2K). Both the ultimate stress to fracture and elastic modulus of GILT$^{-/-}$ tibiae were significantly higher than those of WT samples, suggesting increased bone strength and stiffness (Fig. 2, L and M). Notably, related models of osteopetrosis in adult mice with cathepsin K or V-ATPase deficiencies demonstrate similar increases in bone strength (*34*, *35*). Overall, these data are consistent with an appreciable osteopetrotic phenotype in GILT-deficient mice and point to a nonredundant role for GILT in bone resorption.

GILT deficiency impairs bone resorption by osteoclasts

To assess a potential influence of GILT in the derivation of osteoclasts, the efficiencies of WT and GILT$^{-/-}$ murine monocytic precursors to differentiate into mature osteoclasts in the presence of M-CSF and RANKL were evaluated. After 6 days in culture, WT and GILT$^{-/-}$ samples produced comparable numbers of tartrate-resistant acid phosphatase (TRAP)–positive multinucleated osteoclasts, demonstrating that the absence of GILT did not affect the

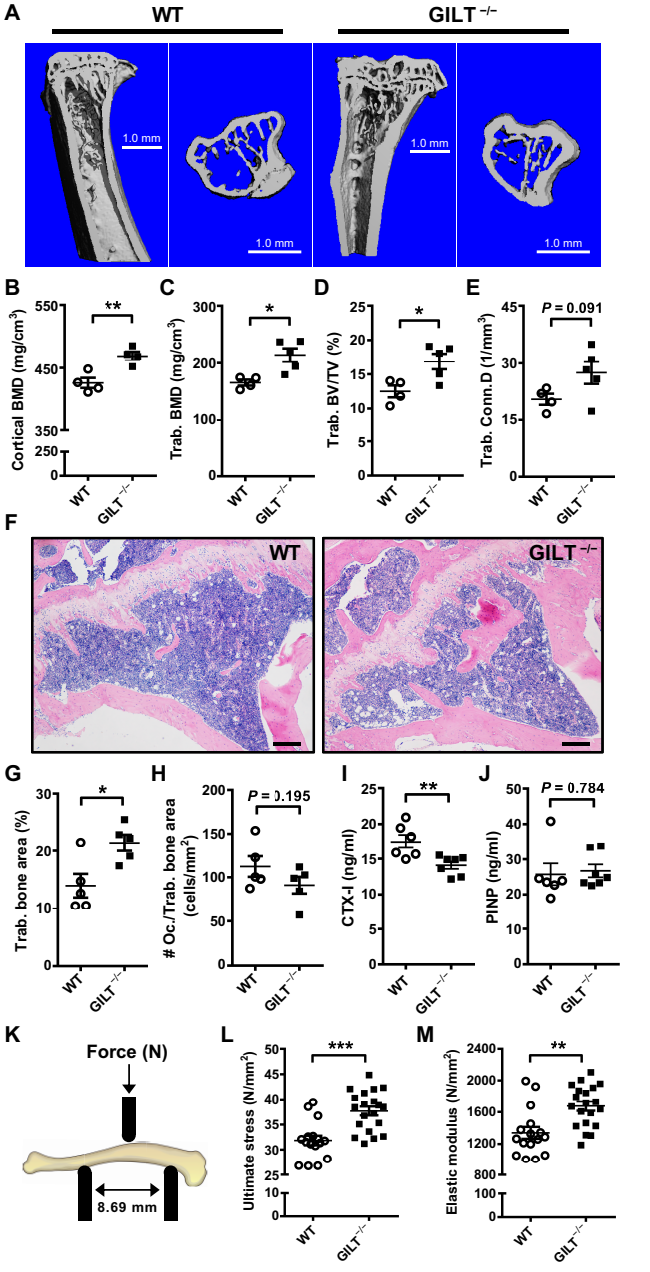

Fig. 2. Tibiae from GILT-deficient mice exhibit osteopetrotic characteristics. (**A**) Representative longitudinal and cross-sectional μCT images of tibiae from 20-week-old female WT or GILT$^{-/-}$ mice. (**B** to **E**) Cortical bone mineral density [cortical BMD (B)], trabecular bone mineral density [Trab. BMD (C)], trabecular bone volume ratio [Trab. BV/TV (D)], and trabecular connective density [Trab. Conn.D (E)] of tibiae from 20-week-old female WT or GILT$^{-/-}$ mice as determined by μCT ($n = 4$ to 5). (**F**) Representative images of proximal tibiae from 20-week-old female WT or GILT$^{-/-}$ mice following hematoxylin and eosin (H&E) staining. Scale bars, 200 μm. (**G** and **H**) Area of trabecular (Trab.) bone per region of interest (G) and numbers of osteoclasts (Oc.) per trabecular bone area (H) from each H&E-stained histological sample ($n = 5$). (**I** and **J**) Serum concentrations of the collagen breakdown product CTX-I (I) and bone formation product PINP (J) measured in 20-week-old female WT or GILT$^{-/-}$ mice ($n = 6$ to 7) (**K**) Schematic representing ex vivo analysis of 20-week-old WT or GILT$^{-/-}$ tibiae using three-point flexural testing. (**L** and **M**) Ultimate stress before fracture (L) and elastic modulus (M) of tibiae as measured by the three-point bend test ($n = 16$ to 20). (B to M) Error bars are presented as means ± SEM. $^{*}P < 0.05$, $^{**}P < 0.01$, $^{***}P < 0.001$ by unpaired Student's *t* test.

differentiation of osteoclasts in vitro (Fig. 3, A and B), corroborating our findings in vivo (Fig. 2H). To determine the efficiency of bone resorption by WT and GILT$^{-/-}$ osteoclasts, monocytic precursors were differentiated into mature osteoclasts on bovine bone slices for 12 days, and resulting areas of resorption were stained with toluidine blue and quantified. GILT-deficient osteoclasts were significantly less efficient in their ability to resorb bone compared with WT osteoclasts (Fig. 3, C and D). Impaired bone resorption by GILT$^{-/-}$ osteoclasts was further demonstrated by scanning electron microscopy (Fig. 3E) and reduced concentrations of the cathepsin K–dependent bone resorption by-product CTX-I (serum C-terminal telopeptide of type I collagen) in the supernatants of bone slices resorbed by GILT$^{-/-}$ osteoclasts (Fig. 3F). In contrast to CTX-I, release of the MMP-dependent collagenolytic by-product ICTP (cross-linked carboxyterminal telopeptide of type I collagen) was equal between WT and GILT$^{-/-}$ osteoclasts (fig. S3) (*36*). The presence of GILT had no discernable influence on the expression and processing patterns of cathepsin K in mature osteoclasts (fig. S4, A to D), nor on the production of reactive oxygen species (fig. S5). Together, these results suggest that GILT deficiency does not affect osteoclastogenesis but confers a defect in osteoclastic bone resorption.

GILT denatures the bone matrix protein SPARC through direct disulfide reduction

Conceivably, disulfide-containing proteins within the organic bone matrix would be susceptible to direct reduction by GILT in the resorption lacuna. Because type I collagen, the main organic constituent of bone tissue, contains no disulfides in its mature fiber structure, we explored the potential for GILT to reduce secreted protein acidic and rich in cysteine (SPARC; also known as osteonectin). SPARC is one of the most abundant noncollagenous proteins in bone and contains seven intramolecular disulfide bonds within its 43-kDa structure that are essential for its role as a structural bone matrix protein (*37*). Principally, SPARC is thought to aid and nucleate bone mineralization with both collagen and hydroxyapatite (HA) crystal binding domains, and its deficiency leads to overt osteopenia in mice (*38*, *39*). To determine whether GILT could directly reduce disulfides in SPARC, active recombinant human GILT was incubated with native human SPARC in a reconstituted system at 37°C, pH 5, with 100 μM cysteine. Following labeling of liberated thiols with biotinylated iodoacetamide and detection by Western blot under nonreducing conditions (Fig. 4A), it was found that incubation with GILT increased the amount of free thiols in SPARC as evidenced by enhanced SPARC biotinylation (Fig. 4B). Reduction by GILT also affected the native structure of SPARC, as reduced SPARC displayed a gel shift as previously described (Fig. 4B) (*40*). Thus, SPARC, a major structural protein within the organic bone matrix, is susceptible to GILT-mediated reduction and subsequent denaturation.

GILT enhances the proteolytic activity of cathepsin K

Similar to SPARC, we found the number of free thiols in recombinant cathepsin K was increased following incubation with active GILT (fig. S6). As with other cysteine cathepsins, the active-site cysteine of cathepsin K must be in a reduced thiol state for proteolytic function, leaving the enzyme susceptible to oxidative inactivation, particularly in acidic environments. We thus measured hydrolysis of a cathepsin K–specific peptide substrate (Abz-HPGGPQ-EDDnp) by human cathepsin K in a reconstituted system with or without active human GILT, hypothesizing that the reductase function of GILT would help maintain the proteolytic capacity of cathepsin K. In agreement with our previous work with cathepsin S (*26*), rates

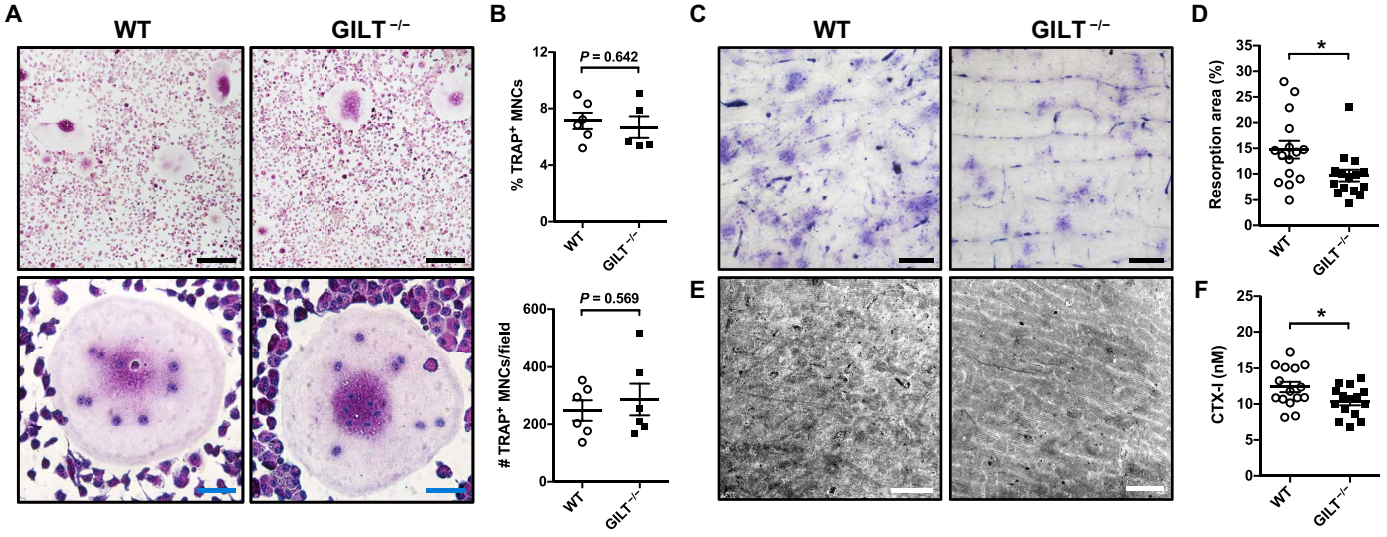

Fig. 3. GILT deficiency results in decreased bone resorption in vitro. (**A**) Representative images of TRAP-stained WT and GILT$^{-/-}$ osteoclasts. (**B**) Enumeration of osteoclastogenesis following RANKL treatment of WT and GILT$^{-/-}$ cells ($n = 5$ to 6 biological replicates). Osteoclasts were defined as TRAP^{+} (purple) multinucleated cells (MNCs; ≥3 nuclei). (A and B) Cells were differentiated using M-CSF (15 ng/ml) and RANKL (100 ng/ml) for 6 days on plastic dishes before TRAP staining. (**C** and **D**) Representative images (C) and quantification (D) of resorption pits on bovine bone slices ($n = 15$ biological replicates). WT and GILT$^{-/-}$ osteoclasts from age- and sex-matched mice were differentiated on top of individual bone slices for 12 days, and resulting resorption pits were stained with toluidine blue for quantification. (**E**) Representative scanning electron microscopy images of resorption pits on bovine bone slices generated by WT (left) or GILT$^{-/-}$ (right) osteoclasts over 12 days. (**F**) Concentrations of the collagen breakdown product CTX-I released from bone slices following 12 days of resorption as measured by ELISA ($n = 15$). (A to F) Scale bars, 500 μm (E, white), 200 μm (A and C, black), or 50 μm (A, blue). Each *n* represents osteoclasts isolated from a single animal. Error bars are presented as means ± SEM. *$P < 0.05$ by unpaired Student's *t* test (B and F) or Mann-Whitney *U* test (D).

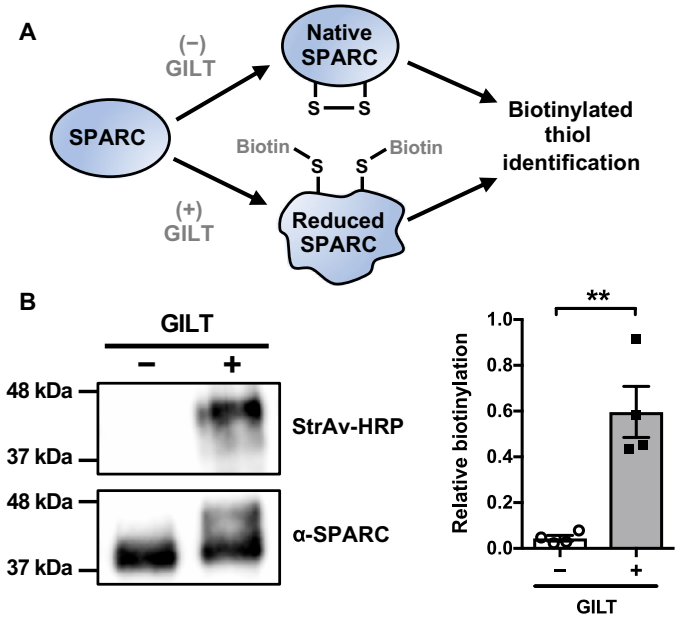

Fig. 4. GILT reduces the noncollagenous bone matrix protein SPARC. (**A**) Schematic representing the biotinylation of liberated free thiols on recombinant SPARC following direct reduction by GILT. (**B**) Representative Western blot image depicting levels of biotinylated SPARC with or without coincubation with bioactive GILT and following labeling of free thiols by the thiol-reactive biotinylation reagent biotin ethylenediamine iodoacetamide. Band intensity of biotinylated SPARC was quantified and made relative to positive control samples treated with 25 mM dithiothreitol (DTT) ($n = 4$ independent experiments). SPARC (500 ng) was diluted in assay buffer (50 mM sodium acetate, 100 μM cysteine, pH 5) with or without GILT (500 ng) and incubated at 37°C for 1 hour before thiol labeling. StrAv-HRP, streptavidin-HRP. Error bars are presented as means ± SEM. $^{**}P < 0.01$ by unpaired Student's t test.

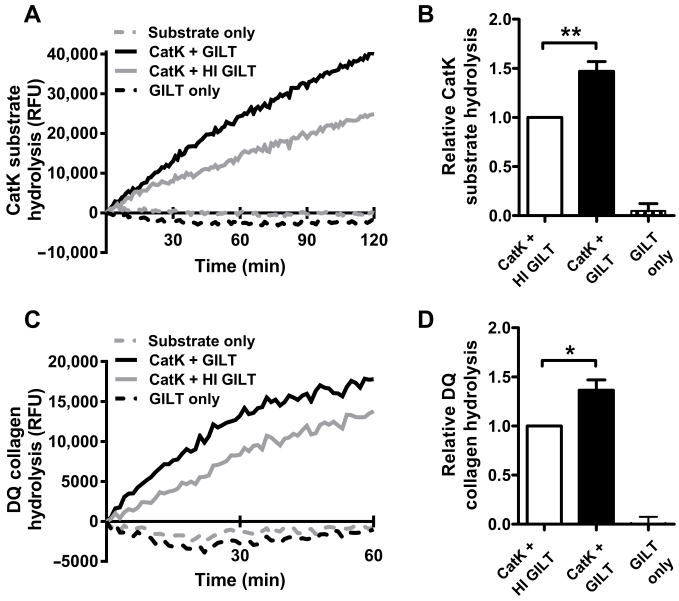

Fig. 5. GILT maintains cathepsin K proteolytic activity in a reconstituted system. (**A** and **C**) Representative real-time kinetic measurement of the hydrolysis of a cathepsin K (CatK)–specific substrate (Abz-HPGGPQ-EDDnp, A) or the collagenase substrate DQ collagen (C) by recombinant human CatK with or without bioactive GILT in a reconstituted system. RFU, relative fluorescent units. (**B** and **D**) Averaged rates of Abz-HPGGPQ-EDDnp hydrolysis (B, $n = 5$ independent experiments) or DQ collagen hydrolysis (D, $n = 4$ independent experiments) relative to heat-inactivated (HI) GILT controls. Relative rates were calculated between 60 and 120 min (B) or between 0 and 30 min (D). (A to D) Reactions were performed in assay buffer (pH 5) with 50 mM sodium acetate and 500 μM cysteine. A GILT:CatK ratio of 5:1 (175:35 ng, A and B) or 2:1 (400:200 ng, C and D) was used for each experiment. Where indicated, heat inactivation of GILT was performed at 95°C for 10 min before addition. Error bars are presented as means ± SEM. $^{*}P < 0.05$, $^{**}P < 0.01$ by one-way analysis of variance with Tukey's post hoc test.

of hydrolysis of the Abz-HPGGPQ-EDDnp substrate by cathepsin K were increased in systems with active GILT compared with heat-inactivated GILT (Fig. 5, A and B). Similarly, cathepsin K–mediated hydrolysis of type I collagen labeled with a self-quenched fluorophore (DQ collagen) was significantly more efficient in the presence of active GILT (Fig. 5, C and D). In the absence of cathepsin K, GILT displayed no direct effects on either fluorogenic substrate. Together, these data show that GILT can maintain the proteolytic function of the collagenase cathepsin K, and provide an additional mechanism by which GILT promotes bone resorption in osteoclasts.

DISCUSSION

The collective findings of this study demonstrate a nonredundant role for the lysosomal thioreductase GILT in the maintenance of optimal bone resorption by osteoclasts. We propose that GILT is highly expressed in osteoclasts in response to RANKL and acts in the resorption lacuna to enhance bone degradation via two synergistic mechanisms: direct reduction of noncollagenous structural proteins such as SPARC, and through maintenance of the collagenase cathepsin K in its reduced, active state (Fig. 6).

The initial rational for this study was based on the prediction that GILT would be expressed in osteoclasts because GILT is constitutively expressed in other monocyte-derived cells such as macrophages (*19*, *31*). Osteoclasts were found not only to express GILT but also to express significantly higher levels of GILT than resting bone marrow macrophages, in line with publicly available microarray datasets (*41*). At both transcriptional and translational levels, cytokine stimulation of monocytic precursors with M-CSF and RANKL significantly increased GILT expression compared with M-CSF alone (Fig. 1). RANKL, a member of the tumor necrosis factor superfamily, initiates a tumor necrosis factor receptor–associated factor 6 (TRAF6)–mediated signaling cascade via stimulation of the RANK receptor on the developing osteoclast's surface. Among others, TRAF6 activates the mitogen-activated protein (MAP) kinase p38, resulting in p38-dependent phosphorylation of S727 within the transactivating domain of the transcription factor STAT1 (*33*, *42*). Of note, IFN-γ–mediated induction of GILT expression is dependent on STAT1 activation, and multiple STAT1-recognition sites are found within the human GILT promoter (*32*). Because S727 phosphorylation by secondary signals [e.g., lipopolysaccharide, tumor necrosis factor–α (TNF-α)] greatly enhances STAT1-dependent signaling during an IFN-γ response (*43*–*45*), RANKL-mediated phosphorylation of STAT1 S727 likely underpins, at least in part, the strong induction of GILT during osteoclastogenesis. Indeed, genetic deletion of STAT1 significantly reduced the capacity of RANKL to drive GILT expression within osteoclast precursors (Fig. 1E). Further supporting this conclusion is the induction of another IFN-γ–inducible protein, MIG (monokine

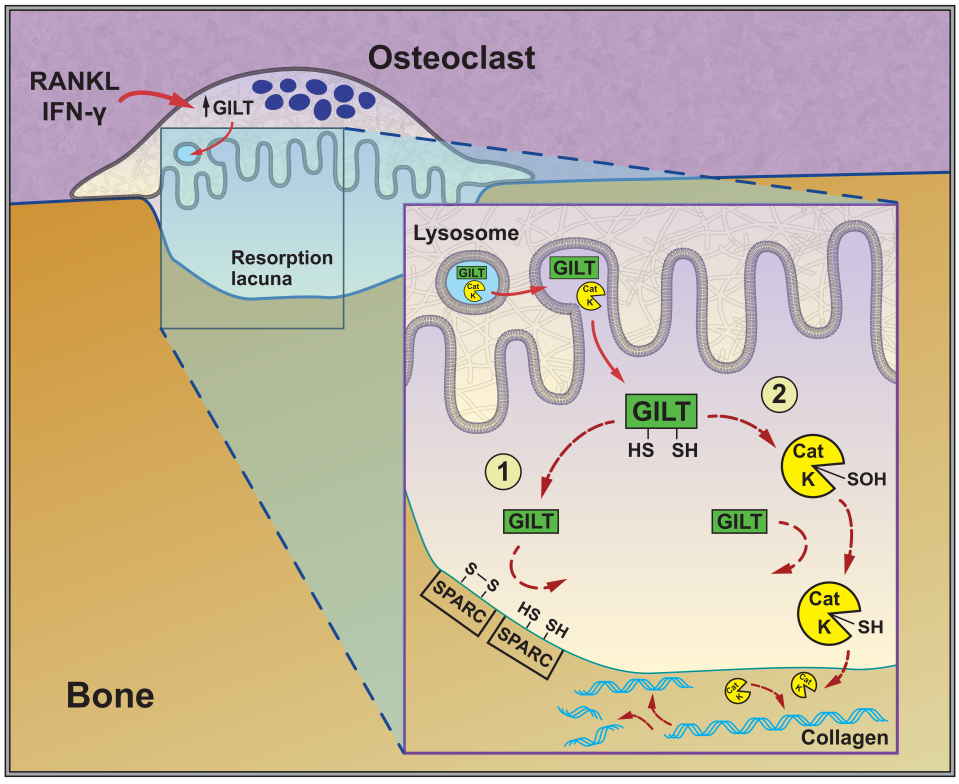

Fig. 6. Proposed mechanisms by which GILT contributes to bone resorption. Increased expression of the lysosomal enzyme GILT in response to RANKL and IFN-γ facilitates accumulation of GILT within the resorption lacuna of the osteoclast. Bone matrix proteins (e.g., SPARC) containing disulfide bonds are consequently susceptible to GILT-mediated reduction and, conceivably, increased proteolytic digestion (mechanism 1, left). In addition, maintenance of cathepsin K (CatK) collagenase activity by GILT promotes increased breakdown of organic bone, improving the overall efficiency of osteoclastic bone resorption (mechanism 2, right).

induced by IFN-γ), in osteoclasts by a RANKL/p38/STAT1-S727–dependent, IFN-γ–independent mechanism (*33*).

Degradation of type I collagen by cathepsin K is a fundamental determinant of bone resorption efficiency (*12*, *14*–*17*, *46*) and suggests the maintenance of cathepsin K activity by GILT (Fig. 5) is at least partially responsible for the impaired bone resorption associated with GILT deficiency in this study. Generation of cathepsin K–dependent, but not MMP-dependent, type I collagen degradation products from bone was found to be impaired in the absence of GILT (Fig. 3F and fig. S3), further emphasizing the role GILT plays in specifically supporting the activities of redox-sensitive cysteine proteases in acidified environments (*36*). While we focused our attention on cathepsin K, the impact of GILT on other cysteine proteases, such as cathepsin S, and other redox-sensitive enzymes within the resorption lacunae of osteoclasts should also be considered. In addition, for GILT to function as a thioreductase, it requires the availability of reductive energy, usually in the form of free cysteine (*18*, *26*, *47*). Whereas the source and forms of reductive equivalents in the osteoclast lacuna have yet to be explored, early studies in the macrophage phagolysosome suggest both exogenous (e.g., extracellular cysteine) and endogenous (e.g., NADPH, selenocysteine-containing reductases) pathways contribute to the reductive capacity of this acidified compartment (*48*). We could predict that reduced cysteine liberated through the degradation of organic bone would provide a source of reducing equivalents within osteoclast lacunae, although similar to the phagolysosome of the macrophage, cytosolic pathways may also contribute.

In addition to reductive maintenance of cathepsin K, we demonstrate that disulfides within the structural bone matrix protein SPARC are susceptible to GILT-mediated reduction (Fig. 4). The presence of numerous disulfide bonds within SPARC is unique among bone matrix glycoproteins (*49*). While the GILT-mediated reduction and degradation of SPARC in vivo were not directly demonstrated and are a limitation of this study, the denaturation of the SPARC tertiary structure by GILT would theoretically destabilize the overall organization of the bone matrix, leaving SPARC increasingly susceptible to proteolytic cleavage. Similar to collagen, SPARC is directly degraded by cathepsin K (*12*, *50*); thus, GILT-mediated reduction of SPARC and activation of cathepsin K may work synergistically to enhance SPARC turnover during bone resorption. Although we focused on SPARC, akin to its demonstrated promiscuity in antigen processing (*51*), GILT is likely to reduce other disulfide-containing, noncollagenous proteins within the resorption lacuna such as the proteoglycan biglycan (*52*), which may influence the physiological and biomechanical properties of bone in GILT-deficient animals. The potentially vast GILT interactome within the osteoclast lacuna could explain the distinct phenotype of adult GILT$^{-/-}$ bones, whereby the increase in bone mineral density is associated with increased bone strength and stiffness, contrasting the brittle bone osteopetrosis seen in human pycnodysostosis (*15*). Nonetheless, related models

of osteopetrosis in adult mice with deficiencies in cathepsin K or V-ATPase have demonstrated similar increases in bone strength (*34*, *35*).

In this study, we found that IFN-γ could further enhance GILT expression in mature murine osteoclasts (fig. S2). Long-term therapy with recombinant IFN-γ greatly improves bone resorption in human patients with severe malignant osteopetrosis (*53*, *54*). Similarly, IFN-γ therapy is effective in increasing bone resorption in several mouse models of osteopetrosis (*55*, *56*). The impact of IFN-γ on osteoclast biology is complicated—in vitro, IFN-γ is widely considered a strong suppresser of osteoclastogenesis (*57*, *58*); however, contradictory findings have been reported depending on the IFN-γ concentration, degree of osteoclast differentiation, and presence of costimulating cytokines (*59*). Stimulated superoxide production by osteoclast precursors (*54*) and activation of T cells to release osteoclastogenic RANKL and TNF-α (*57*) are proposed mechanisms for enhanced bone resorption in response to IFN-γ in humans and mice, respectively; however, augmentation of GILT expression in osteoclasts presents a plausible parallel mechanism. Further investigation into the role of GILT during IFN-γ therapy, and bone remodeling in general, is warranted and may support the use of GILT-related therapeutic strategies for bone disease.

Seminal discoveries by others have identified key, nonredundant roles for GILT in adaptive immunity, and as such, GILT has been primarily considered an enzyme of the immune system (*18*, *21*–*24*, *60*, *61*). The existence of GILT homologs in a variety of primitive species that lack adaptive immune systems, however, suggests that GILT-like thiol oxidoreductases evolved to perform critical roles outside of antigen processing (*27*, *28*, *30*). This study identifies such a role for GILT in the homeostasis of bone. Given the widespread physiological necessity to reduce disulfides and maintain cysteine protease activities in acidic environments, we anticipate that GILT will continue to emerge as a critical enzyme for many biological processes spanning many species.

MATERIALS AND METHODS

Mice

C57BL/6 (WT) and B6.129S(Cg)-*Stat1*^{tm1Dlv}/J (STAT1$^{-/-}$) mice were purchased from the Jackson laboratory (*62*). Congenic C57BL/6 GILT$^{-/-}$ (GILT$^{-/-}$) mice were provided by P. Cresswell (Yale University School of Medicine) (*23*). All animals received identical husbandry within the Clara Christie Centre for Mouse Genomics (University of Calgary). Mouse experiments were performed according to protocols approved by the University of Calgary Animal Use and Care Committee and designed in accordance with the Canadian Council for Animal Care. Age- and sex-matched participants were used within each experiment. For in vivo μCT, 20-week-old female mice were euthanized and frozen at −20°C before analysis.

Osteoclast culture

Bone marrow cells were flushed from the tibia, femur, and ilium of 6- to 8-week-old WT or GILT$^{-/-}$ mice. Following red blood cell lysis (4 min, 155 mM NH_4Cl, 12 mM $NaHCO_3$, and 0.1 mM EDTA) and filtration (70 μm), cells were cultured in T-25 flasks overnight in basal media [10% fetal bovine serum, penicillin-streptomycin (100 U/ml), 2 mM L-glutamine, and 1 mM sodium pyruvate in DMEM] with recombinant M-CSF (15 ng/ml). Resulting nonadherent precursor cells were plated at 5×10^4 cells per well (96-well plate with or without bone slices; Fig. 3 and fig. S3), 2×10^5 cells per well (24-well plate; Fig. 1C), or 1×10^6 cells per well (6-well plate; Fig. 1, A and B, and figs. S2 and S4) with M-CSF (15 ng/ml) for 24 hours. Subsequently, fresh osteoclast media [M-CSF (15 ng/ml) and RANKL (100 ng/ml)] or control media [M-CSF (15 ng/ml) only] was added. Both macrophages and osteoclasts received stimulation with M-CSF (15 ng/ml) through the entirety of each experiment. Cells were differentiated for 6 [quantitative polymerase chain reaction (qPCR), Western blot, immunofluorescence, and TRAP staining] or 12 (bone slice experiments) additional days, with half-media changes performed every 2 days. For 12-day bone slice experiments, only quarter-media changes were performed on days 8 and 10 to help maintain supernatant CTX-I and ICTP concentrations. To assess the effect of IFN-γ on osteoclastic GILT expression, fully differentiated osteoclasts at day 6 were treated with IFN-γ (500 U/ml) for 24 hours before total RNA or protein isolation. Osteoclastogenesis was confirmed by TRAP staining using the Acid Phosphatase, Leukocyte kit (Sigma-Aldrich) according to the manufacturer's recommendations. Cells were imaged with an Olympus IX71 inverted microscope using an Olympus DP72 digital color camera. For the purpose of enumeration, osteoclasts were defined as TRAP$^+$, multinucleated cells (≥3 nuclei), and two randomized 4× fields of view were counted and averaged for cells from each biological replicate.

STAT1 signaling

WT or STAT1$^{-/-}$ nonadherent precursor cells (isolated as described above) were plated at 5×10^5 cells per well (12-well plate; Fig. 1, D and E) with M-CSF (15 ng/ml) for 48 hours to produce homogeneous monocytic populations. To evaluate STAT1 phosphorylation (Fig. 1D), WT cells were first cultured in low-serum media (0.1% fetal bovine serum) overnight, and then either left untreated, treated with RANKL (200 ng/ml) (15 min), or treated with IFN-γ (100 U/ml) (15 min) immediately before lysis and Western blot analysis. Alternatively, WT or STAT1$^{-/-}$ cells were stimulated with M-CSF (15 ng/ml) or M-CSF and RANKL (15 ng/ml and 100 ng/ml, respectively) for an additional 48 hours followed by Western blot analysis to evaluate the involvement of STAT1 during early induction of GILT expression (Fig. 1E).

Quantitative polymerase chain reaction

Total RNA was extracted using an RNeasy Mini Kit (Qiagen) and quantified by NanoDrop analysis (Thermo Fisher Scientific). qScript cDNA Supermix (Quanta BioSciences) was used for cDNA synthesis, and iQ Supermix (Bio-Rad) was used for qPCR amplification. Reactions were run on an iQ5 thermocycler (Bio-Rad) under the following conditions: 95°C for 3 min, followed by 50 cycles of 95°C for 30 s and 58°C for 30 s. All primers were designed using Primer3 as follows: GILT (gene name: *IFI30*, forward: 5′-CTGTTCCCACTCGAGGTTCC-3′, reverse: 5′-CCATCACCATCAGCCAGGTT-3′); cathepsin K (gene name: *CTSK*, forward: 5′-CTTTGGAAGGGAGTGGGCAT-3′, reverse: 5′-ACCAGCACAGAGTCCACAAC-3′); TRAP (gene name: *ACP5*, forward: 5′-AAAATGCCTCGAGACCTGGG-3′, reverse: 5′-GTAGGCAGTGACCCCGTATG-3′); 18*S* (forward: 5′-CGCGGTTCTATTTTGTTGGT-3′, reverse: 5′-AGTCGGCATCGTTTATGGTC-3′). All products displayed a single melt curve, and each gene was normalized to 18*S* ribosomal RNA as an internal control. Biological replicates were tested under each experimental condition and made relative, and the results were paired for statistical analysis.

Western blot

Cells were lysed on ice for 10 min with ice-cold lysis buffer [1% NP-40, 150 mM NaCl, and 50 mM tris (pH 8)]. For STAT1 phosphorylation blots (Fig. 1D), cells were lysed using radioimmunoprecipitation assay buffer [0.1% SDS, 1% Triton X-100, 1 mM EDTA, 150 mM NaCl, and 25 mM tris (pH 7.5)] containing 1× protease/phosphatase inhibitor (Cell Signaling Technologies). Lysates were centrifuged at 10,000*g* for 10 min, and supernatants were transferred to fresh tubes. Samples were prepared in SDS sample buffer, with (reducing; Fig. 1 and figs. S2 and S4) or without (nonreducing; Fig. 4 and fig. S6) β-mercaptoethanol, and boiled for 5 min before loading. Total GILT expression was measured using a mouse α-mouse GILT primary antibody (clone MaP.mGILT6, Hycult Biotech) (*63*) followed by a horse α-mouse immunoglobulin G (IgG)–horseradish peroxidase (HRP) secondary antibody (#7076, Cell Signaling Technology). Cell lysates were run on Mini-PROTEAN TGX Stain-Free protein gels (Bio-Rad), and expression of mature GILT was normalized to total protein levels using Image Lab software (Bio-Rad). Rabbit α-mouse P-S727 STAT1 (#9177), P-Y701 STAT1 (#9167), and total STAT1 (#9172) antibodies (all Cell Signaling Technologies) were used to evaluate STAT1 signaling and were probed using a goat α-rabbit IgG-HRP secondary antibody (#7074, Cell Signaling Technology). Following P-S727 and P-Y701 detection, blots were stripped and probed for total STAT1, and P-S727 and P-Y701 levels were normalized to total STAT1 protein levels. Cathepsin K expression was measured using a rabbit α-cathepsin K primary antibody (ab19027, Abcam) followed by a goat α-rabbit IgG-HRP secondary antibody. Cathepsin K expression was normalized to the housekeeping gene glyceraldehyde-3-phosphate dehydrogenase (GAPDH) (using rabbit α-GAPDH primary antibody #2118, Cell Signaling Technologies). Biotinylated SPARC and biotinylated cathepsin K were probed using Precision Protein Strep-Tactin HRP Conjugate (Bio-Rad). Equal SPARC loading was confirmed using goat α-human SPARC (AF941, R&D Systems) followed by a donkey α-goat IgG-HRP secondary antibody (sc-2020, Santa Cruz Biotechnology). Equal cathepsin K loading was confirmed using rabbit α-cathepsin K (ab19027, Abcam) followed by a goat α-rabbit IgG-HRP secondary antibody.

Immunofluorescence

Cells plated on glass coverslips were fixed for 15 min with 4% paraformaldehyde. After extensive washing with phosphate-buffered saline (PBS), cells were permeabilized with 0.1% Triton X-100 for 15 min, and coverslips were blocked with 5% goat serum/1% bovine serum albumin for 1 hour at room temperature. Samples were incubated with primary antibodies overnight at 4°C, including mouse α-mouse GILT (clone MaP.mGILT6, Hycult Biotech) (*63*) and rabbit α-mouse cathepsin K (ab19027, Abcam). Following PBS washes, secondary antibodies [Alexa Fluor 488 goat α-mouse IgG (A11029) and Alexa Fluor 594 goat α-rabbit IgG (A11037), Thermo Fisher Scientific] and Phalloidin-iFluor 647 (ab176759, Abcam) were added to each coverslip for 1 hour at room temperature. Last, nuclei were stained with Bisbenzimide H 33258 (VWR) (1 μg/ml) for 10 min in the dark, and coverslips were mounted on microscope slides using Dako Fluorescence Mounting Medium (Agilent). Cells were imaged on an Olympus IX71 inverted epifluorescence microscope using a Retiga 2000R CCD digital camera (QImaging). Specificity of the α-GILT antibody was confirmed using cells from GILT$^{-/-}$ mice, and no-primary controls were performed to assess nonspecific binding of secondary antibodies. Colocalization of GILT and cathepsin K signals was assessed using the JACoP colocalization plugin for ImageJ (*64*) to calculate Pearson's correlation coefficient, a measure of linear association, across entire BMMØ or osteoclast images. Costes' automatic threshold method was used to minimize background fluorescence.

Microcomputed tomography

Frozen euthanized mice were thawed overnight at 4°C and then brought to room temperature. The proximal 6.36 mm of the right limb of each mouse was scanned using a vivaCT 40 scanner (Scanco Medical) under the following conditions as previously described (*65*): isotropic resolution, 15 μm; tube voltage, 45 kVp; tube current, 133 μA; and integration time, 200 ms. Scans consisted of 1000 projections over 180° and were reconstructed on a 2048 × 2048 matrix. Calibration of the scanner was performed using HA phantoms. Subsequent to the scans, Image Processing Language (IPL V5.08b, Scanco Medical) was used to extract the trabecular and cortical regions of the tibiae via segmentation. The mean gray scale values of voxels in both the trabecular and cortical regions were converted to mg of HA/cm^3 and reported individually as trabecular and cortical bone mineral density. Trabecular bone volume ratio (BV/TV) and trabecular connectivity density (Conn.D) were calculated after segmentation.

Three-point flexural test

After μCT scanning, the mice were dissected, and their tibiae harvested. The samples were wrapped in gauze dipped in PBS and frozen at −20°C until further use. The day of the biomechanical tests, samples were thawed to room temperature, and both left and right tibiae underwent three-point bending analysis using an ElectroForce 3200 test instrument (Bose Corporation) as previously described (*66*). Briefly, the lateral surface of the tibia was placed on the bending jig with lower supports located 8.69 mm apart at the tibial crest and the tibia-fibula junction. Tibiae were stabilized by applying a 1-newton preload to the midpoint between the two lower supports. Subsequently, load was applied and measured using a 450-newton load cell at a displacement rate of 0.033 mm/s. Force was applied to the bone until fracture, and force values in newtons were normalized to the geometry of the bone to calculate flexural stress ($\sigma = 3PL/2bd^2$, where P is the applied load in newtons, L is the span length of 8.69 mm, b is the tibia width, and d is the tibia depth). Strength of each bone was quantified as the ultimate stress reached before fracture. Elastic modulus, a measure of resistance to elastic deformation under stress, was calculated by plotting stress (σ) versus strain ($\varepsilon = 6Dd/L^2$, where D is the displacement in millimeters, d is the tibia depth, and L is the span length) and calculating the maximal slope of the linear region with an $R^2 \geq 0.995$.

Bone histomorphometry

Tibiae were isolated from 20-week-old WT and GILT$^{-/-}$ mice and fixed overnight in 10% buffered formalin at room temperature. Bones were washed in PBS, and then decalcified for 1 week in ddH_2O with 10% EDTA at room temperature. Bones were sectioned in series longitudinally at 3 μm in paraffin and stained with hematoxylin and eosin (Prairie Diagnostic Services). Sections were imaged with an Olympus IX71 inverted microscope (4× fields of view) using an Olympus DP72 digital color camera and subsequently analyzed for trabecular bone area and osteoclast numbers using cellSens image analysis software (Olympus). Histopathological assessment was performed by an American College of Veterinary Pathology–certified pathologist (A.L.W.) in a blinded fashion. Regions of interest for measuring trabecular bone area and osteoclast

counts were defined using the cortical bone and growth plate as boundaries.

Bone resorption assay

Bovine bone slices (Immunodiagnostic Systems) were stained for areas of resorption as previously described (*67*). Briefly, supernatants from wells containing bone slices were collected for CTX-I and ICTP analyses, and the bone slices were washed twice with PBS followed by 1 N NaOH for 30 s to remove cellular content. After three additional washes with distilled water, bone slices were removed from each well and left to air dry. Bone slices were stained with 1% toluidine blue in 1% sodium borate for 5 min, followed by three successive rinses with distilled water. Once air dried, bone slices were imaged with an Olympus IX71 inverted microscope using an Olympus DP72 digital color camera. Areas of resorption were defined as pits/trenches positively stained with toluidine blue, and percentages of resorption within each total area were quantified using ImageJ. Two unrelated 4× fields of view representing maximal levels of bone resorption were quantified and averaged for each bone slice, with each bone slice representing osteoclasts from an individual biological replicate. For scanning electron microscopy, representative bone slices previously resorbed by WT or GILT$^{-/-}$ osteoclasts were loaded onto copper tape and sputter coated with gold-palladium before visualization using an XL30 scanning electron microscope (Philips).

Enzyme-linked immunosorbent assay

CTX-1 and PINP concentrations in 20-week-old female WT or GILT$^{-/-}$ mice were determined using a RatLaps (CTX-I) EIA Immunoassay (Immunodiagnostic Systems) and a Rat/Mouse PINP EIA Immunoassay (Immunodiagnostic Systems), respectively, according to the manufacturer's instructions. Fasting blood samples were collected by cardiac puncture, centrifuged at 300*g* for 15 min to remove cellular content, transferred to fresh tubes, and stored at −80°C before analysis. Cell culture concentrations of CTX-I and ICTP were determined using a CrossLaps for Culture (CTX-I) ELISA (enzyme-linked immunosorbent assay) Immunoassay (Immunodiagnostic Systems) and a Bovine ICTP Competitive ELISA kit (MyBioSource), respectively, according to the manufacturer's instructions. Collected supernatants from resorbed bone slices were centrifuged at 300*g* for 15 min and stored at −80°C until CTX-I/ICTP analysis. For all ELISA assays, samples were run in duplicate and averaged, and concentrations were interpolated from a sigmoidal four parameter logistic (4-PL) curve-fit standard curve.

H_2O_2 quantification

The generation of extracellular hydrogen peroxide (H_2O_2) by WT and GILT$^{-/-}$ osteoclasts was assessed using the redox-sensitive reagent Amplex UltraRed (Thermo Fisher Scientific). Nonadherent osteoclast precursor cells were plated at high density (2.5×10^5 cells per well; 96-well plate) and differentiated into osteoclasts using M-CSF (15 ng/ml) and RANKL (100 ng/ml) for 6 days, as described above. The following day, 150 µl of osteoclast supernatant (or media-only control) was transferred to a fresh 96-well plate and incubated with 10 µM Amplex UltraRed reagent and HRP (2 U/ml) (Sigma-Aldrich) in the dark for 30 min at room temperature. The absolute fluorescence intensity of the resulting oxidized product (resorufin) was measured using an EnVision Multilabel Plate Reader (PerkinElmer).

Recombinant GILT reductase activity

Recombinant human GILT expressed in human embryonic kidney (HEK) 293 cells (LS-G50826) was purchased from LifeSpan BioSciences. To confirm reductase bioactivity of the GILT enzyme (see fig. S7, A and B), the disulfide-containing fluorogenic cystine-based reagent BODIPY FL L-cystine (Thermo Fisher Scientific) was diluted to a final concentration of 5 µM in assay buffer (50 mM sodium acetate, 200 µM cysteine, pH 5). Subsequently, 200 ng of GILT, 200 ng of heat inactivated GILT (enzyme heat inactivated at 95°C for 10 min before addition), or no GILT was added to the reaction mixture at a final total volume of 50 µl, and fluorescence liberation was kinetically measured in real time at 37°C for 180 min using a FLUOstar OPTIMA microplate reader (BMG Labtech). Following the subtraction of background fluorescence (samples with 5 µM substrate in assay buffer, no cysteine), rates of disulfide reduction were determined by calculating the slope of the real-time trace between 45 and 90 min ($y = mx + c$, where y is the relative fluorescence, m is the slope, and x is the time) and made relative to the no GILT control.

Free thiol labeling and quantification

We diluted 500 ng of recombinant human SPARC (PeproTech) or 200 ng of recombinant human cathepsin K (EMD Millipore) in assay buffer (50 mM sodium acetate, 100 µM cysteine, pH 5) with or without the addition of 500 ng of recombinant human GILT (LifeSpan BioSciences) at a final reaction volume of 30 µl, and the reaction mixture was incubated at 37°C for 1 hour. GILT (or vehicle) was preactivated with 50 µM dithiothreitol (DTT) (15 min, 37°C) before addition. Identical samples containing excess DTT (25 mM) were also prepared as a positive control for disulfide reduction. To both quench the reaction and label newly liberated thiols, biotin ethylenediamine iodoacetamide (Biotium) in 10× borate-buffered saline (pH 8.8) was added to each reaction mix to a final concentration of 250 µM. The labeling reaction was performed in the dark for 90 min at room temperature, and final products were quenched with nonreducing SDS sample buffer before separation by SDS–polyacrylamide gel electrophoresis. Protein bands corresponding to biotinylated SPARC were analyzed using Image Lab software (Bio-Rad), and band intensity was made relative to 25 mM DTT-positive controls.

Recombinant cathepsin K activity assays

Maintenance of cathepsin K proteolytic activity by GILT was measured using a protocol adapted from our previous study with cathepsin S (*26*). Briefly, 35 ng (Fig. 5, A and B) or 200 ng (Fig. 5, C and D) of recombinant human cathepsin K (ab157067, Abcam) was diluted in assay buffer (50 mM sodium acetate, 500 µM cysteine, pH 5). Subsequently, recombinant human GILT (LS-Bio) or heat inactivated (HI) GILT (enzyme heat inactivated at 95°C for 10 min before addition) was added to the reaction at a 5:1 ratio (175 ng GILT; Fig. 5, A and B) or a 2:1 ratio (400 ng GILT; Fig. 5, C and D). Recombinant GILT activity was previously demonstrated to be completely heat labile (*26*), with heat-inactivated GILT having no effect on cathepsin activity in an acidic reconstituted system (see fig. S7, C and D). GILT and heat-inactivated GILT were pretreated with 50 µM DTT (15 min, 37°C) before addition. Immediately before commencing measurements, 50 µM of the fluorescent cathepsin K–specific substrate Abz-HPGGPQ-EDDnp (Anaspec) or 60 µg/ml of the fluorescent collagenase substrate DQ collagen (type I, Thermo Fisher Scientific) was added to each reaction mixture to a final total volume of 50 µl. Proteolytic cleavage of each substrate

was kinetically measured in real time at 37°C using a FLUOstar OPTIMA microplate reader (BMG Labtech). Following the subtraction of background fluorescence (samples containing substrate in assay buffer), rates of proteolysis were determined by calculating the slope of the real-time trace between 60 and 120 min (Fig. 5, A and B) or between 0 and 30 min (Fig. 5, C and D) ($y = mx + c$, where y is the relative fluorescence, m is the slope, and x is the time) and made relative to heat-inactivated GILT samples.

Statistical analysis

All statistical analyses were completed using Prism software (GraphPad). Analyses were performed using a two-tailed Student's t test or one-way analysis of variance with a multiple comparison analysis (Tukey's post hoc test). Nonparametric results were analyzed using a two-tailed Mann-Whitney U test. Outliers as identified by Grubbs' test ($P < 0.05$) were excluded ($n = 1$ each for Figs. 1A, 2B, and 3, B and F). Where indicated, paired statistics were used for experimental conditions arising from the same biological replicate. $P < 0.05$ was considered statistically significant. The specific statistical test used and number of replicates for each experiment are outlined in the appropriate figure legends.

SUPPLEMENTARY MATERIALS

Supplementary material for this article is available at http://advances.sciencemag.org/cgi/content/full/7/17/eabd3684/DC1

View/request a protocol for this paper from *Bio-protocol*.

REFERENCES AND NOTES

1. X. Feng, J. M. McDonald, Disorders of bone remodeling. *Annu. Rev. Pathol.* **6**, 121–145 (2011).
2. C. Sobacchi, A. Schulz, F. P. Coxon, A. Villa, M. H. Helfrich, Osteopetrosis: Genetics, treatment and new insights into osteoclast function. *Nat. Rev. Endocrinol.* **9**, 522–536 (2013).
3. S. Gordon, P. R. Taylor, Monocyte and macrophage heterogeneity. *Nat. Rev. Immunol.* **5**, 953–964 (2005).
4. C. E. Jacome-Galarza, G. I. Percin, J. T. Muller, E. Mass, T. Lazarov, J. Eitler, M. Rauner, V. K. Yadav, L. Crozet, M. Bohm, P. L. Loyher, G. Karsenty, C. Waskow, F. Geissmann, Developmental origin, functional maintenance and genetic rescue of osteoclasts. *Nature* **568**, 541–545 (2019).
5. S. L. Teitelbaum, Bone resorption by osteoclasts. *Science* **289**, 1504–1508 (2000).
6. Y. Yahara, T. Barrientos, Y. J. Tang, V. Puviindran, P. Nadesan, H. Zhang, J. R. Gibson, S. G. Gregory, Y. Diao, Y. Xiang, Y. J. Qadri, T. Souma, M. L. Shinohara, B. A. Alman, Erythromyeloid progenitors give rise to a population of osteoclasts that contribute to bone homeostasis and repair. *Nat. Cell Biol.* **22**, 49–59 (2020).
7. W. J. Boyle, W. S. Simonet, D. L. Lacey, Osteoclast differentiation and activation. *Nature* **423**, 337–342 (2003).
8. D. L. Lacey, E. Timms, H. L. Tan, M. J. Kelley, C. R. Dunstan, T. Burgess, R. Elliott, A. Colombero, G. Elliott, S. Scully, H. Hsu, J. Sullivan, N. Hawkins, E. Davy, C. Capparelli, A. Eli, Y. X. Qian, S. Kaufman, I. Sarosi, V. Shalhoub, G. Senaldi, J. Guo, J. Delaney, W. J. Boyle, Osteoprotegerin ligand is a cytokine that regulates osteoclast differentiation and activation. *Cell* **93**, 165–176 (1998).
9. R. Baron, L. Neff, W. Brown, P. J. Courtoy, D. Louvard, M. G. Farquhar, Polarized secretion of lysosomal enzymes: Co-distribution of cation-independent mannose-6-phosphate receptors and lysosomal enzymes along the osteoclast exocytic pathway. *J. Cell Biol.* **106**, 1863–1872 (1988).
10. R. Baron, L. Neff, D. Louvard, P. J. Courtoy, Cell-mediated extracellular acidification and bone resorption: Evidence for a low pH in resorbing lacunae and localization of a 100-kD lysosomal membrane protein at the osteoclast ruffled border. *J. Cell Biol.* **101**, 2210–2222 (1985).
11. H. C. Blair, S. L. Teitelbaum, R. Ghiselli, S. Gluck, Osteoclastic bone resorption by a polarized vacuolar proton pump. *Science* **245**, 855–857 (1989).
12. M. J. Bossard, T. A. Tomaszek, S. K. Thompson, B. Y. Amegadzie, C. R. Hanning, C. Jones, J. T. Kurdyla, D. E. McNulty, F. H. Drake, M. Gowen, M. A. Levy, Proteolytic activity of human osteoclast cathepsin K: Expression, purification, activation, and substrate identification. *J. Biol. Chem.* **271**, 12517–12524 (1996).
13. H. Zhao, Y. Ito, J. Chappel, N. W. Andrews, S. L. Teitelbaum, F. P. Ross, Synaptotagmin VII regulates bone remodeling by modulating osteoclast and osteoblast secretion. *Dev. Cell* **14**, 914–925 (2008).
14. F. H. Drake, R. A. Dodds, I. E. James, J. R. Connor, C. Debouck, S. Richardson, E. Lee-Rykaczewski, L. Coleman, D. Rieman, R. Barthlow, G. Hastings, M. Gowen, Cathepsin K, but not cathepsins B, L, or S, is abundantly expressed in human osteoclasts. *J. Biol. Chem.* **271**, 12511–12516 (1996).
15. B. D. Gelb, G. P. Shi, H. A. Chapman, R. J. Desnick, Pycnodysostosis, a lysosomal disease caused by cathepsin K deficiency. *Science* **273**, 1236–1238 (1996).
16. M. Gowen, F. Lazner, R. Dodds, R. Kapadia, J. Feild, M. Tavaria, I. Bertoncello, F. Drake, S. Zavarselk, I. Tellis, P. Hertzog, C. Debouck, I. Kola, Cathepsin K knockout mice develop osteopetrosis due to a deficit in matrix degradation but not demineralization. *J. Bone Miner. Res.* **14**, 1654–1663 (1999).
17. P. Saftig, E. Hunziker, O. Wehmeyer, S. Jones, A. Boyde, W. Rommerskirch, J. D. Moritz, P. Schu, K. von Figura, Impaired osteoclastic bone resorption leads to osteopetrosis in cathepsin-K-deficient mice. *Proc. Natl. Acad. Sci. U.S.A.* **95**, 13453–13458 (1998).
18. B. W. Ewanchuk, R. M. Yates, The phagosome and redox control of antigen processing. *Free Radic. Biol. Med.* **125**, 53–61 (2018).
19. B. Arunachalam, U. T. Phan, H. J. Geuze, P. Cresswell, Enzymatic reduction of disulfide bonds in lysosomes: Characterization of a gamma-interferon-inducible lysosomal thiol reductase (GILT). *Proc. Natl. Acad. Sci. U.S.A.* **97**, 745–750 (2000).
20. U. T. Phan, B. Arunachalam, P. Cresswell, Gamma-interferon-inducible lysosomal thiol reductase (GILT). Maturation, activity, and mechanism of action. *J. Biol. Chem.* **275**, 25907–25914 (2000).
21. C. M. Bergman, C. B. Marta, M. Maric, S. E. Pfeiffer, P. Cresswell, N. H. Ruddle, A switch in pathogenic mechanism in myelin oligodendrocyte glycoprotein-induced experimental autoimmune encephalomyelitis in IFN-γ–inducible lysosomal thiol reductase-free mice. *J. Immunol.* **188**, 6001–6009 (2012).
22. M. A. Haque, P. Li, S. K. Jackson, H. M. Zarour, J. W. Hawes, U. T. Phan, M. Maric, P. Cresswell, J. S. Blum, Absence of gamma-interferon-inducible lysosomal thiol reductase in melanomas disrupts T cell recognition of select immunodominant epitopes. *J. Exp. Med.* **195**, 1267–1277 (2002).
23. M. Maric, B. Arunachalam, U. T. Phan, C. Dong, W. S. Garrett, K. S. Cannon, C. Alfonso, L. Karlsson, R. A. Flavell, P. Cresswell, Defective antigen processing in GILT-free mice. *Science* **294**, 1361–1365 (2001).
24. R. Singh, P. Cresswell, Defective cross-presentation of viral antigens in GILT-free mice. *Science* **328**, 1394–1398 (2010).
25. M. Yang, C. Haase, J. Viljanen, B. Xu, C. Ge, J. Kihlberg, R. Holmdahl, Cutting edge: Processing of oxidized peptides in macrophages regulates T cell activation and development of autoimmune arthritis. *J. Immunol.* **199**, 3937–3942 (2017).
26. D. R. Balce, E. R. O. Allan, N. McKenna, R. M. Yates, γ-interferon-inducible lysosomal thiol reductase (GILT) maintains phagosomal proteolysis in alternatively activated macrophages. *J. Biol. Chem.* **289**, 31891–31904 (2014).
27. N. Liu, S. Zhang, Z. Liu, S. Gaowa, Y. Wang, Characterization and expression of gamma-interferon-inducible lysosomal thiol reductase (GILT) gene in amphioxus *Branchiostoma belcheri* with implications for GILT in innate immune response. *Mol. Immunol.* **44**, 2631–2637 (2007).
28. U. T. Phan, M. Maric, T. P. Dick, P. Cresswell, Multiple species express thiol oxidoreductases related to GILT. *Immunogenetics* **53**, 342–346 (2001).
29. M. P. Rausch, K. T. Hastings, Diverse cellular and organismal functions of the lysosomal thiol reductase GILT. *Mol. Immunol.* **68**, 124–128 (2015).
30. L. C. West, P. Cresswell, Expanding roles for GILT in immunity. *Curr. Opin. Immunol.* **25**, 103–108 (2013).
31. A. D. Luster, R. L. Weinshank, R. Feinman, J. V. Ravetch, Molecular and biochemical characterization of a novel gamma-interferon-inducible protein. *J. Biol. Chem.* **263**, 12036–12043 (1988).
32. P. W. O'Donnell, A. Haque, M. J. Klemsz, M. H. Kaplan, J. S. Blum, Cutting edge: Induction of the antigen-processing enzyme IFN-gamma-inducible lysosomal thiol reductase in melanoma cells Is STAT1-dependent but CIITA-independent. *J. Immunol.* **173**, 731–735 (2004).
33. H. B. Kwak, S. W. Lee, H. M. Jin, H. Ha, S. H. Lee, S. Takeshita, S. Tanaka, H.-M. Kim, H.-H. Kim, Z. H. Lee, Monokine induced by interferon-gamma is induced by receptor activator of nuclear factor kappa B ligand and is involved in osteoclast adhesion and migration. *Blood* **105**, 2963–2969 (2005).
34. K. Henriksen, C. Flores, J. S. Thomsen, A.-M. Brüel, C. S. Thudium, A. V. Neutzsky-Wulff, G. E. J. Langenbach, N. Sims, M. Askmyr, T. J. Martin, V. Everts, M. A. Karsdal, J. Richter, Dissociation of bone resorption and bone formation in adult mice with a non-functional V-ATPase in osteoclasts leads to increased bone strength. *PLOS ONE* **6**, e27482 (2011).
35. B. Pennypacker, M. Shea, Q. Liu, P. Masarachia, P. Saftig, S. Rodan, G. Rodan, D. Kimmel, Bone density, strength, and formation in adult cathepsin K (–/–) mice. *Bone* **44**, 199–207 (2009).

36. P. Garnero, M. Ferreras, M. A. Karsdal, R. Nicamhlaoibh, J. Risteli, O. Borel, P. Qvist, P. D. Delmas, N. T. Foged, J. M. Delaissé, The type I collagen fragments ICTP and CTX reveal distinct enzymatic pathways of bone collagen degradation. *J. Bone Miner. Res.* **18**, 859–867 (2003).
37. E. Hohenester, P. Maurer, R. Timpl, Crystal structure of a pair of follistatin-like and EF-hand calcium-binding domains in BM-40. *EMBO J.* **16**, 3778–3786 (1997).
38. J. D. Termine, H. K. Kleinman, S. W. Whitson, K. M. Conn, M. L. McGarvey, G. R. Martin, Osteonectin, a bone-specific protein linking mineral to collagen. *Cell* **26**, 99–105 (1981).
39. A. M. Delany, M. Amling, M. Priemel, C. Howe, R. Baron, E. Canalis, Osteopenia and decreased bone formation in osteonectin-deficient mice. *J. Clin. Invest.* **105**, 915–923 (2000).
40. L. Cheng, E. H. Sage, Q. Yan, SPARC fusion protein induces cellular adhesive signaling. *PLOS ONE* **8**, e53202 (2013).
41. J. E. Lattin, K. Schroder, A. I. Su, J. R. Walker, J. Zhang, T. Wiltshire, K. Saijo, C. K. Glass, D. A. Hume, S. Kellie, M. J. Sweet, Expression analysis of G protein-coupled receptors in mouse macrophages. *Immunome Res.* **4**, 5 (2008).
42. M. Matsumoto, T. Sudo, T. Saito, H. Osada, M. Tsujimoto, Involvement of p38 mitogen-activated protein kinase signaling pathway in osteoclastogenesis mediated by receptor activator of NF-κ B ligand (RANKL). *J. Biol. Chem.* **275**, 31155–31161 (2000).
43. P. Kovarik, D. Stoiber, P. A. Eyers, R. Menghini, A. Neininger, M. Gaestel, P. Cohen, T. Decker, Stress-induced phosphorylation of STAT1 at Ser727 requires p38 mitogen-activated protein kinase whereas IFN-γ uses a different signaling pathway. *Proc. Natl. Acad. Sci. U.S.A.* **96**, 13956–13961 (1999).
44. P. Kovarik, D. Stoiber, M. Novy, T. Decker, Stat1 combines signals derived from IFN-gamma and LPS receptors during macrophage activation. *EMBO J.* **17**, 3660–3668 (1998).
45. Z. Wen, Z. Zhong, J. E. Darnell Jr., Maximal activation of transcription by Stat1 and Stat3 requires both tyrosine and serine phosphorylation. *Cell* **82**, 241–250 (1995).
46. P. Garnero, O. Borel, I. Byrjalsen, M. Ferreras, F. H. Drake, M. S. McQueney, N. T. Foged, P. D. Delmas, J. M. Delaissé, The collagenolytic activity of cathepsin K is unique among mammalian proteinases. *J. Biol. Chem.* **273**, 32347–32352 (1998).
47. C. S. Pillay, E. Elliott, C. Dennison, Endolysosomal proteolysis and its regulation. *Biochem. J.* **363**, 417–429 (2002).
48. D. R. Balce, C. J. Greene, P. Tailor, R. M. Yates, Endogenous and exogenous pathways maintain the reductive capacity of the phagosome. *J. Leukoc. Biol.* **100**, 17–26 (2016).
49. A. L. Boskey, Noncollagenous matrix proteins and their role in mineralization. *Bone Miner.* **6**, 111–123 (1989).
50. I. Podgorski, B. E. Linebaugh, J. E. Koblinski, D. L. Rudy, M. K. Herroon, M. B. Olive, B. F. Sloane, Bone marrow-derived cathepsin K cleaves SPARC in bone metastasis. *Am. J. Pathol.* **175**, 1255–1269 (2009).
51. B. Bogunovic, P. Srinivasan, Y. Ueda, Y. Tomita, M. Maric, Comparative quantitative mass spectrometry analysis of MHC class II-associated peptides reveals a role of GILT in formation of self-peptide repertoire. *PLOS ONE* **5**, e10599 (2010).
52. T. Xu, P. Bianco, L. W. Fisher, G. Longenecker, E. Smith, S. Goldstein, J. Bonadio, A. Boskey, A. M. Heegaard, B. Sommer, K. Satomura, P. Dominguez, C. Zhao, A. B. Kulkarni, P. G. Robey, M. F. Young, Targeted disruption of the biglycan gene leads to an osteoporosis-like phenotype in mice. *Nat. Genet.* **20**, 78–82 (1998).
53. L. L. Key Jr., W. L. Ries, R. M. Rodriguiz, H. C. Hatcher, Recombinant human interferon gamma therapy for osteopetrosis. *J. Pediatr.* **121**, 119–124 (1992).
54. L. L. Key Jr., R. M. Rodriguiz, S. M. Willi, N. M. Wright, H. C. Hatcher, D. R. Eyre, J. K. Cure, P. P. Griffin, W. L. Ries, Long-term treatment of osteopetrosis with recombinant human interferon gamma. *N. Engl. J. Med.* **332**, 1594–1599 (1995).
55. I. Alam, A. K. Gray, D. Acton, R. L. Gerard-O'Riley, A. M. Reilly, M. J. Econs, Interferon gamma, but not calcitriol improves the osteopetrotic phenotypes in ADO2 mice. *J. Bone Miner. Res.* **30**, 2005–2013 (2015).
56. R. M. Rodriguiz, L. L. Key Jr., W. L. Ries, Combination macrophage-colony stimulating factor and interferon-gamma administration ameliorates the osteopetrotic condition in microphthalmic (mi/mi) mice. *Pediatr. Res.* **33**, 384–389 (1993).
57. Y. Gao, F. Grassi, M. R. Ryan, M. Terauchi, K. Page, X. Yang, M. N. Weitzmann, R. Pacifici, IFN-gamma stimulates osteoclast formation and bone loss in vivo via antigen-driven T cell activation. *J. Clin. Invest.* **117**, 122–132 (2007).
58. H. Takayanagi, K. Ogasawara, S. Hida, T. Chiba, S. Murata, K. Sato, A. Takaoka, T. Yokochi, H. Oda, K. Tanaka, K. Nakamura, T. Taniguchi, T-cell-mediated regulation of osteoclastogenesis by signalling cross-talk between RANKL and IFN-γ. *Nature* **408**, 600–605 (2000).
59. M. Tang, L. Tian, G. Luo, X. Yu, Interferon-gamma-mediated osteoimmunology. *Front. Immunol.* **9**, 1508 (2018).
60. R. Singh, A. Jamieson, P. Cresswell, GILT is a critical host factor for Listeria monocytogenes infection. *Nature* **455**, 1244–1247 (2008).
61. L. C. West, J. E. Grotzke, P. Cresswell, MHC class II-restricted presentation of the major house dust mite allergen Der p 1 Is GILT-dependent: Implications for allergic asthma. *PLOS ONE* **8**, e51343 (2013).
62. J. E. Durbin, R. Hackenmiller, M. C. Simon, D. E. Levy, Targeted disruption of the mouse Stat1 gene results in compromised innate immunity to viral disease. *Cell* **84**, 443–450 (1996).
63. R. L. Lackman, A. M. Jamieson, J. M. Griffith, H. Geuze, P. Cresswell, Innate immune recognition triggers secretion of lysosomal enzymes by macrophages. *Traffic* **8**, 1179–1189 (2007).
64. S. Bolte, F. P. Cordelieres, A guided tour into subcellular colocalization analysis in light microscopy. *J. Microsc.* **224**, 213–232 (2006).
65. P. Premnath, B. Jorgenson, R. Hess, P. Tailor, D. Louie, J. Taiani, S. Boyd, R. Krawetz, $p21^{-/-}$ mice exhibit enhanced bone regeneration after injury. *BMC Musculoskelet. Disord.* **18**, 435 (2017).
66. C. S. Bahney, D. P. Hu, A. J. Taylor, F. Ferro, H. M. Britz, B. Hallgrimsson, B. Johnstone, T. Miclau, R. S. Marcucio, Stem cell-derived endochondral cartilage stimulates bone healing by tissue transformation. *J. Bone Miner. Res.* **29**, 1269–1282 (2014).
67. A. Vesprey, W. Yang, Pit assay to measure the bone resorptive activity of bone marrow-derived osteoclasts. *Bio-Protoc.* **6**, e1836 (2016).

Acknowledgments

Funding: This study was supported by grants to R.M.Y. from the Natural Sciences and Engineering Research Council of Canada (NSERC) and the Canadian Institutes of Health Research (CIHR). Graduate student support for B.W.E. was provided by NSERC and the Snyder Institute for Chronic Diseases. **Author contributions:** B.W.E., D.R.B., and R.M.Y. conceived and designed the study; B.W.E., C.R.A., D.R.B., P.P., and T.L.O. performed the research; B.W.E., C.R.A., P.P., T.L.O., A.O., and A.L.W. interpreted and analyzed the data; R.J.K. contributed reagents/analytical tools; and B.W.E. and R.M.Y. wrote and revised the manuscript. **Competing interests:** The authors declare that they have no competing interests. **Data and materials availability:** All data needed to evaluate the conclusions in the paper are present in the paper and/or the Supplementary Materials. Additional data related to this paper may be requested from the authors.

Submitted 21 June 2020
Accepted 5 March 2021
Published 23 April 2021
10.1126/sciadv.abd3684

Citation: B. W. Ewanchuk, C. R. Arnold, D. R. Balce, P. Premnath, T. L. Orsetti, A. L. Warren, A. Olsen, R. J. Krawetz, R. M. Yates, A non-immunological role for γ-interferon–inducible lysosomal thiol reductase (GILT) in osteoclastic bone resorption. *Sci. Adv.* **7**, eabd3684 (2021).